Gb3-binding lectins as potential carriers for transcellular drug delivery

Stefan K. Müller, Isabel Wilhelm, Thomas Schubert, Katharina Zittlau, Anne Imberty, Josef Madl, Thorsten Eierhoff, Roland Thuenauer, Winfried Römer

Gb3-binding lectins as potential carriers for transcellular drug delivery

Stefan K. Müller[a,b], Isabel Wilhelm[a,b], Thomas Schubert[a,b], Katharina Zittlau[a,b], Anne Imberty[c], Josef Madl[a,b], Thorsten Eierhoff[a,b], Roland Thuenauer[a,b,*], Winfried Römer[a,b,*]

[a] Faculty of Biology, Albert-Ludwigs-University Freiburg, Schänzlestraße 1, 79104 Freiburg, Germany
[b] BIOSS – Centre for Biological Signalling Studies, Albert-Ludwigs-University Freiburg, Schänzlestraße 18, 79104 Freiburg, Germany
[c] Centre de Recherches sur les Macromolécules Végétales, UPR5301 CNRS and University of Grenoble Alpes, BP53, 38041 Grenoble cédex 09, France

* To whom correspondence should be addressed:

Jun.-Prof. Dr. Winfried Römer
Albert-Ludwigs-University Freiburg, BIOSS Centre for Biological Signalling Studies, Schänzlestraβe 18, Germany.
Phone: +49 (0)761 203 67500
E-mail: winfried.roemer@bioss.uni-freiburg.de

Dr. Roland Thuenauer
Albert-Ludwigs-University Freiburg, BIOSS Centre for Biological Signalling Studies, Schänzlestraβe 18, Germany.
Phone: +49 (0)761 203 67505
E-mail: roland.thuenauer@gmail.com

Abstract

Cellular barriers like the blood-brain barrier (BBB) drastically reduce the efficiency of targeted drug delivery. In this study we investigated lectins that are able to bind the glycosphingolipid globotriaosylceramide (Gb3) for their potential as carriers for transcytotic drug delivery. In particular, we utilized the B-subunit of Shiga toxin (StxB), and LecA, which is produced by the bacterium *Pseudomonas aeruginosa*. We found that both lectins were rapidly transcytosed in an *in vitro* model of the BBB based on Madin Darby canine kidney (MDCK) cells transfected with Gb3 synthase. Transcytosis occurred from the apical to the basolateral plasma membrane and *vice versa*. The first step in transcytosis was the internalization into early endosomes from the side from which the lectins were applied. Whereas StxB proceeded on both, the retrograde and the transcytotic transport route, LecA avoided the retrograde transport route. This differential trafficking could be explained by our observation that the two lectins segregated into distinct membrane domains already during endocytosis. Furthermore, transcytosis of both lectins from the basolateral to the apical side was completely blocked by inhibiting the small GTPase Rab11a through overexpression of dominant negative Rab11a-S25N in MDCK cells. Since Rab11a organizes trafficking at the level of apical recycling endosomes (ARE), this suggests that ARE are a central hub from which apical delivery occurs during basolateral to apical transcytosis. Taken together, our data demonstrates that glycosphingolipid-binding lectins are promising candidates for trans-BBB drug delivery. Our findings show that lectins with structurally different binding pockets for the same glycosphingolipid receptor can take different intracellular trafficking routes. This indicates that there is the possibility to enhance transcellular drug delivery by utilizing carrier lectins that are engineered to take specific trafficking pathways.

Keywords

apical recycling endosome, Rab GTPase, LecA, polarized cells, Shiga toxin, transcytosis

1 Introduction

In the human body, the blood stream is separated from the rest of the tissue by monolayers of endothelial cells. These cellular barriers represent a major challenge for drug delivery from the blood stream into organs, where most drugs act on specific targets. One notable example is the blood-brain barrier (BBB). During recent years an increasing number of promising drug candidates were developed to treat neuropathological diseases and intracranial neoplasms. However, these drugs have to overcome the BBB to act directly on the central nervous system (CNS) [1]. The BBB itself is built by endothelial cells lining the blood capillaries of the brain [2,3]. Its main functions are to protect the CNS against invasion of toxic and infectious agents and to ensure an appropriate salt concentration in the extravascular space [3]. The BBB is an exceptionally leak-proof barrier and prevents the passage of more than 98 % of small molecule-based drugs and nearly all large molecule-based drugs from the bloodstream to the CNS [1]. The tightness of the BBB results from many BBB-specific features: First, fenestrae, which allow trans-endothelial transport in other types of endothelia, are missing in the BBB [1,4]. Second, individual BBB cells are linked by very dense tight junctions (TJs), which almost completely block paracellular transport [5]. Third, endothelial cells of the BBB express several efflux pumps, like the P-glycoprotein, which actively pump drug molecules from the cytosol back to the bloodstream [6–9].

Nevertheless, diffusion-based drug delivery remains the predominant approach for the majority of drugs utilized today [10]. In order to compensate for low diffusion efficiencies, this approach requires the administration of high drug doses to ensure that sufficient concentrations reach the target site. In further consequence, this requires additional effort in drug design to minimize off-target effects. An alternative approach is receptor-mediated drug delivery [4,11]. In this strategy, endogenous transcytotic transport pathways are utilized. The drug is coupled to a suitable ligand that binds to an endogenous host cell receptor on the luminal side of the BBB, which faces the blood stream. The drug-ligand-receptor complex undergoes transcytosis, which results in transport of the drug to the abluminal side facing the CNS. Most transcytotic transport routes that have been suggested for trans-BBB drug delivery rely on proteinaceous receptors, such as the transferrin receptor [12,13] and insulin receptor [4,14,15]. In these cases, the drug carrier has either to compete with endogenous ligands, or when carriers structurally non-related to ligands are used, might still be limited by the default transcytosis rate of endogenous receptor-ligand complexes.

An interesting alternative strategy is to utilize glycosphingolipids as carriers for transcytotic drug delivery. First, glycosphingolipids show a very high default transcytosis rate [16,17], and second, there exist several glycosphingolipid-specific lectins that can additionally force their own uptake by forming plasma membrane invaginations [18].

In this study, we investigated whether two lectins that bind the glycosphingolipid globotriaosylceramide (also called Gb3, CD77 or Pk blood group antigen), which is expressed in endothelia [19–21], can be utilized as carriers for transcytotic drug delivery. The first lectin was the B-subunit of Shiga toxin (StxB), which is a homo-pentameric protein that can bind up to 15 Gb3 molecules [22,23], whereas the second lectin, LecA from *Pseudomonas aeruginosa* [24] is a homo-tetramer that contains 4 Gb3 binding sites [25]. We found that StxB as well as LecA are rapidly transcytosed across model cellular barriers formed by Madin Darby canine kidney (MDCK) cells [6,8] that have been transfected with Gb3 synthase. Transcytosis occurred in both directions, from the apical to basolateral side and *vice versa*, with almost similar kinetics. Whereas StxB underwent transcytosis as well as retrograde trafficking to the Golgi apparatus, LecA did only marginally appear at the Golgi apparatus. In line with this observation, the two lectins were seen to segregate already during endocytosis into separate membrane domains. Moreover, we demonstrate that functional Rab11a, which is a small GTPase organizing trafficking at the level of apical recycling endosomes (ARE) [26–28], is required for apical delivery during StxB and LecA transcytosis from the basolateral to the apical side.

2 Materials and Methods

2.1 Cell culture

MDCK II cells, kindly provided by E. Rodriguez-Boulan (Weill Cornell Medical College), were cultivated in Dulbecco's modified Eagle's medium (DMEM) (Invitrogen), supplemented with 5 % fetal bovine serum (FBS) (Invitrogen) at 37°C and 5 % CO_2. Generation of MDCK II cells stably expressing Gb3 synthase (MDCK $Gb3^+$) was performed as described recently [24]. Briefly, wild-type (wt) MDCK II cells were transfected with a plasmid encoding for Gb3 synthase and G418 resistance. Next, cells were selected with 1 mg/ml G418 for 2 weeks and surviving clones were isolated. A clone showing homogenous and high Gb3 expression and ability to form well-polarized monolayers (assayed by comparing the trans-epithelial electrical resistance (TEER) to that of wt MDCK II cell monolayers) was chosen and utilized for further experiments.

To obtain *in vitro* model barriers, we seeded $3*10^5$ cells on Transwell filters (Corning, #3401), and cultivated the cells for four days. To obtain monolayers that contain only single or small colonies of $Gb3^+$ cells surrounded by wt cells, we mixed trypsinized and resuspended wt MDCK II cells with $Gb3^+$ MDCK cells in a ratio 10:1 before seeding. To ensure sufficient monolayer tightness, only monolayers showing a TEER > 210 $\Omega*cm^2$ were used for experiments.

2.2 Bioconjugation of biotin and fluorescent dyes to lectins

We utilized NHS-ester-functionalized biotin, Alexa488, Cy3, and Alexa647 (ThermoFisher) for bioconjugation to the purified lectins StxB (Sigma-Aldrich) as well as LecA [25]. For the labelling reactions, the following molar ratios were used: 1:10 for $StxB_{monomer}$:biotin, 1:20 for $LecA_{monomer}$:biotin, and 1:5 for $StxB_{monomer}$:fluorophores and $LecA_{monomer}$:fluorophores. Labelling was carried out for 1 h at room temperature (RT) in phosphate-buffered saline (PBS) (Invitrogen) supplemented with 10 mM $NaCO_3$ (pH 8.2). For double-labelling of StxB with fluorophores and biotin, biotin conjugation was carried out first, followed by conjugation with fluorophores (ratio 1:5 for $StxB_{monomer}$-biotin:fluorophores). Purification of labelled proteins was done with Slide-a-Lyzer™ dialysis cassettes (ThermoScientific).

2.3 Transcytosis assay

To measure transcytosis, 150 µl of complete medium supplemented with 4 µg/ml of StxB-biotin-Alexa488 or 6 µg/ml of LecA-biotin was applied to either the apical or basolateral compartment of Transwell filter-grown MDCK monolayers for 30 min at 4°C. After

removing unbound lectin by washing with chilled medium, transcytosis was initiated by heating the cells to 37°C. After the desired time periods, trafficking was stopped by applying chilled medium. To detect transcytosed lectins, 150 µl of medium supplemented with 2 µg/ml streptavidin-Alexa647 was applied at the opposite compartment of the initial lectin application for 30 min at 4°C. Next, cells were washed twice at the side at which streptavidin-Alexa647 had been applied, and then twice at both sides with PBS supplemented with $CaCl_2$ and $MgCl_2$ ($PBS^{+/+}$) (Invitrogen). Then, cells were fixed for 15 min at 4°C and then for 15 min at RT in PBS supplemented with 4% paraformaldehyde (PFA). Fixation was stopped by washing with PBS containing 50 mM NH_4Cl. After three washes with PBS, cells were incubated with SAPO buffer (PBS supplemented with 0.2% bovine serum albumin, 0.02% saponin, and 0.5 µg/ml DAPI) for 30 min at RT. When lectins tagged only with biotin were used, total lectins were counter-stained by incubation with 2 µg/ml streptavidin-Alexa488 in SAPO for 1 h at RT.

After mounting of cells in a glycerol solution supplemented with 1,4-diazabicyclo[2.2.2]octane (DABCO) [29], at least 50 $Gb3^+$ cells per condition were imaged with a confocal fluorescence microscope (Nikon A1R equipped with an 60x oil immersion objective (N.A. 1.49) and laser lines at 405 nm, 488 nm, 561 nm and 647 nm). To quantify the amount of transcytosed and totally bound and uptaken lectin, the corresponding intensities were measured from individual cells by analyzing the confocal data with a custom-written Matlab program.

2.4 Co-localization assays

To examine intracellular compartments implicated in transcytosis of LecA and StxB, cell culture medium supplemented with 4 µg/ml of StxB-Cy3 or 6 µg/ml LecA-Cy3 was utilized. The experimental procedure was similar as for the transcytosis assays. However, after cells were heated to 37°C for 0 to 120 min to enable transcytosis, samples were washed once with pre-chilled medium and twice with pre-chilled $PBS^{+/+}$ before they were fixed and permeabilized with SAPO. Intracellular compartments were then stained by applying primary antibodies dissolved in SAPO (5 µg/ml mouse anti-EEA1 (# E41120, BD Transduction Laboratories) to stain early endosomes (EE), 5 µg/ml rabbit anti-Rab11 (# 71-5300, Invitrogen) to stain ARE, 5 µg/ml mouse anti-giantin (# ab37266, Abcam) to stain the Golgi apparatus) for 1 h at RT followed by incubation with appropriate secondary antibodies dissolved in SAPO (10 µg/ml anti-mouse-Alexa488 (# A21202, Invitrogen), and 10 µg/ml anti-rabbit-DyLight650 (# 84546, ThermoScientific) for 30 min at RT. Then, cells were washed three times with PBS and mounted for fluorescence microscopy

analysis. At least 30 $Gb3^+$ cells per condition were imaged with a confocal fluorescence microscope. To quantify co-localization, the Manders coefficient m1 [30], which represents the fraction of the lectin signal that co-localizes with a compartment marker, was determined by analyzing the confocal data with a custom-written Matlab program.

2.5 Inhibition of Rab11a

Rab11a was inhibited by transient co-transfection of polarized wt MDCK cells with dominant negative Rab11a tagged with mCherry (Rab11a-S25N-mCherry) [29] as well as Gb3-synthase [24]. Transfection was carried out using Lipofectamine 2000 (Invitrogen) for 6 h. Subsequently, the transfection solution was removed and cells were incubated for further 3 h in complete medium to ensure sufficient expression of Rab11a-S25N-mCherry before transcytosis assays were started.

2.6 LecA and StxB internalization assays

$Gb3^+$ MDCK II cells were seeded on glass bottom dishes and cultured for 1 day to 10 - 20 % confluency. Then, LecA-Alexa488 (6 µg/ml) and StxB-Alexa647 (4 µg/ml) were pre-bound to the cells for 30 min at 4°C and unbound lectins were washed out. After internalization for 0, 2, and 15 min at 37°C, cells were fixed with PBS supplemented with 4% PFA. Cells were imaged at a confocal microscope after one wash with PBS supplemented with 50 mM NH_4Cl and two washes with PBS.

2.7 Statistical analysis

All results are expressed as mean ± standard error of the mean (SEM) calculated from at least three independent experiments. Statistical significance was analyzed by one-way analysis of variance (ANOVA) followed by Bonferroni's post hoc test.

3 Results

3.1 StxB is rapidly transcytosed from the apical to the basolateral plasma membrane

We investigated the receptor-mediated transcytosis kinetics of StxB by using a temperature-controlled transcytosis assay. We pre-bound StxB-biotin-Alexa488 at 4°C to the apical surface of Transwell filter-grown monolayers of polarized MDCK cells. In order to allow unbiased quantification of signals from individual cells, the monolayers contained only a low amount of isolated $Gb3^+$ MDCK cells that were surrounded by Gb3-negative wt MDCK cells. After removing of unbound lectins by washing, we shifted the temperature to 37°C for periods of 0 to 120 min to enable lectin internalization and intracellular transport. Following this, transcytosed lectin appearing on the basolateral surface was detected by applying streptavidin-Alexa647 to the basolateral side of live cells. In this assay, the 0 min sample served as internal tightness control for the cell monolayer. Since in this sample no transcytosis to the basolateral side could have occurred, any signal detected from streptavidin-Alexa647 labelling would have indicated leakage of the monolayer. To quantify transcytosis, we imaged the samples with a confocal fluorescence microscope, and representative apico-basal cross-sections of individual $Gb3^+$-cells are shown in Fig. 1a. Signal from transcytosed StxB was clearly detectable after 30 min of transport. Transcytosis increased significantly for later points (Fig. 1b).

In addition, we quantified the total amount of StxB-biotin-Alexa488 within the same cells by measuring the signal intensity from the 488-channel (Fig. 1c). With this, we could calculate a transcytosis (pseudo-)efficiency (Fig. 1d) by dividing the signal from the 647-channel (transcytosed StxB) by the signal from the 488-channel (total StxB) for each cell. Due to the different brightnesses of Alexa488 and Alexa647 and unknown labelling efficiencies of StxB-biotin-Alexa488 and streptavidin-Alexa647, the values given in Fig. 1d do not represent the real fraction of StxB undergoing transcytosis. However, these (pseudo-)efficiencies allow relative comparison within one experiment, showing that the transcytosis efficiency saturated after approximately 60 min (Fig. 1d). Furthermore, StxB remained bound to the cells after appearing at the basolateral surface. This indicates that transcytosis occurred exclusively via vesicular transport. All other scenarios would require a transport of StxB across the lipid bilayer, which is highly unlikely for a protein with a molecular weight like StxB (7.7 kDa for a StxB-monomer).

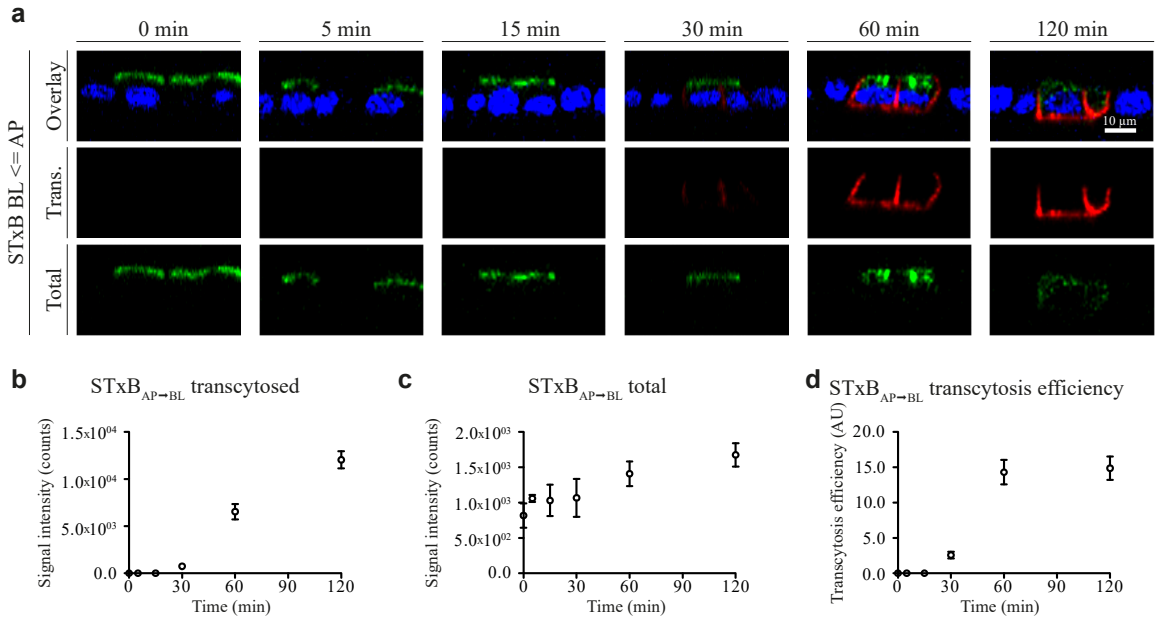

Figure 1: Apically applied StxB is transported to the basolateral plasma membrane via transcytosis.
(a) StxB-biotin-Alexa488 (green) was pre-bound to the apical (AP) plasma membrane at 4°C for 30 min. Then, the cells were shifted to 37°C for the indicated time periods, and StxB arriving at the basolateral (BL) plasma membrane was visualized by staining with streptavidin-Alexa647 (red). After fixation and permeabilization, nuclei were stained with DAPI (blue), and imaged with a confocal microscope. Representative apico-basal cross-sections of $Gb3^+$ MDCK cells surrounded by wt MDCK cells are shown.
(b) – (d) Time course of transcytosed StxB determined from the signal of basolateral surface staining with streptavidin-Alexa647 (b), total StxB obtained from the signal of StxB-biotin-Alexa488 (c) and the transcytosis efficiency calculated from the ratio of surface staining signal to the total StxB signal (d). To calculate the time courses, signals from at least 30 cells per condition were quantified from the microscopy data. The graphs show the average from three independent experiments, the error bars represent the SEM.

3.2 The transcytotic route of StxB from the apical to the basolateral plasma membrane

To study the transcytotic trafficking route of StxB we investigated the co-localization of StxB with intracellular compartment markers. In these assays, StxB-Cy3 was pre-bound to the apical plasma membrane at 4°C, followed by heating to 37°C to enable transcytosis, similarly as described before. After fixation, compartments of interest were marked with appropriate primary and fluorescently labelled secondary antibodies. To quantify co-localization, confocal microscopy was utilized to acquire z-stacks of images to reconstruct three-dimensional representations of the samples. With a custom-written Matlab program, we calculated the Manders co-localization coefficient m1 from the three-dimensional data, which gives the exact proportion of StxB signal co-localizing with a compartment marker.

Internalized StxB was first seen to co-localize with EE (Figs. 2a and S1), which have been visualized by staining with an antibody recognizing the early endosomal antigen 1 (EEA1) [31]. The co-localization between StxB and EEA1 peaked after 15 min of internalization (Fig. 2a). The co-localization with Rab11, a marker of ARE [32–35], reached its apex shortly after, at around 15 - 30 min of internalization (Figs. 2b and S2). These observations indicate that StxB is taken up and enters the apical recycling system that is formed by EE and ARE [27,34,36]. StxB is well known to undergo retrograde transport to the Golgi apparatus and the endoplasmic reticulum (ER) in many cell lines [35,37,38]. Therefore, we investigated the co-localization of internalized StxB with giantin as a marker for the cis- and medial-Golgi apparatus. As depicted in Figs. 2c and S3, StxB reached the Golgi apparatus within 60 min and then co-localization between StxB and giantin saturated. The arrival of StxB at the Golgi (Fig. 2c) occurred concurrently with its arrival at the basolateral plasma membrane after transcytosis (Fig. 1c). This suggests that a fraction of StxB undergoes transcytosis, whereas another fraction is transported in along a retrograde route. As assessed from the value of the co-localization coefficient after 60 min of transport (Fig. 2c), approximately 50% of StxB is transported retrogradely and is therefore not available for transcytosis.

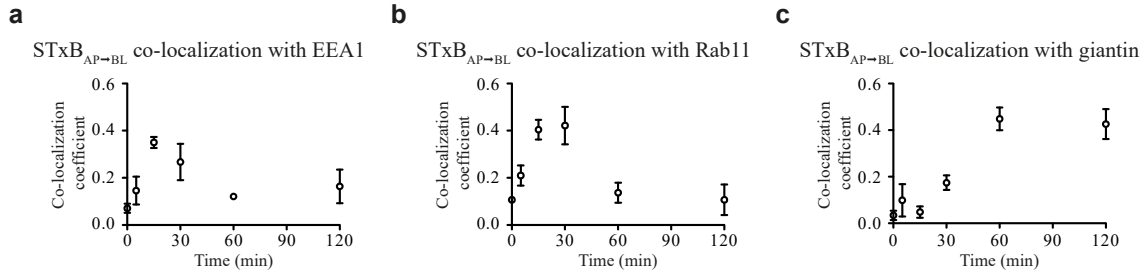

Figure 2: Intracellular trafficking of apically applied StxB.
StxB-Cy3 was pre-bound to the apical (AP) surface at 4°C for 30 min. Then, trafficking was enabled by heating to 37°C for the indicated time periods. After fixation, the cells were co-stained for compartment markers (EEA1 as marker for early endosomes in (a), Rab11 as marker for apical recycling endosomes in (b), and giantin as marker for the cis- and medial-Golgi apparatus in (c)). Representative confocal images for each condition are shown in Figs. S1 - S3, respectively. The Manders co-localization coefficient m1, which represents the fraction of StxB co-localizing with a compartment marker, was quantified with a custom-written Matlab program. The graphs show the time courses of the averaged co-localization coefficients from $n \geq 3$ individual experiments, the error bars represent the SEM.

3.3 StxB is also transcytosed from the basolateral to the apical plasma membrane

By using our transcytosis assay, we also investigated transcytosis of StxB in the basolateral to apical direction (Fig. 3). The quantification revealed that $Gb3^+$ cells expressed on average a lower amount of Gb3 at the basolateral plasma membrane ((2.25 ± 0.46) * 10^2 counts signal intensity from bound StxB at 0 min, Fig. 3c) than on the apical plasma membrane ((8.17 ± 1.71) * 10^2 counts signal intensity from bound StxB at 0 min, Fig. 1c). Nevertheless, transcytosis from the basolateral to the apical plasma membrane was clearly detectable after 30 min of transport (Figs. 3a and 3b). The transcytosis efficiency, calculated as ratio from the signal of transcytosed StxB (Fig. 3b) and totally internalized StxB (Fig. 3c), reached detectable values after 30 min, increased until 60 min, and then decreased again after 120 min (Fig. 3d). This decrease might be due to re-internalization of already transcytosed StxB from the apical plasma membrane.

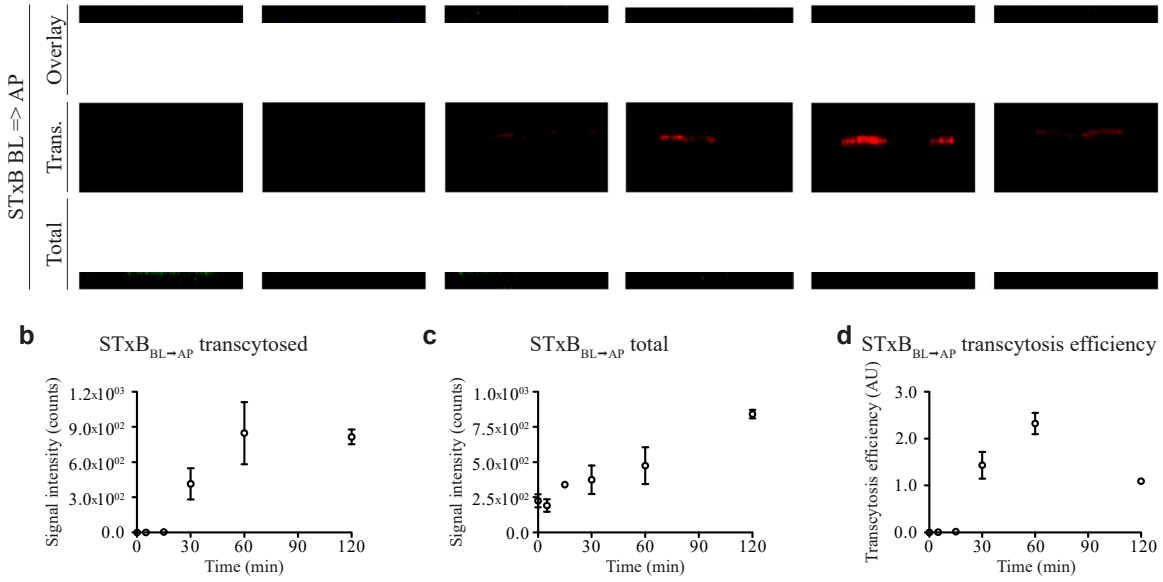

Figure 3: Basolaterally applied StxB is transported to the apical plasma membrane by transcytosis.

(a) StxB-biotin-Alexa488 (green) was pre-bound to the basolateral (BL) plasma membrane for 30 min at 4°C before the cells were incubated at 37°C for the indicated time periods. The arrival of StxB at the apical (AP) plasma membrane was visualized by staining with streptavidin-Alexa647 (red). After fixation and permeabilization of cells, the nuclei (blue) were stained by DAPI followed by imaging with a confocal microscope. Representative apico-basal cross-sections of $Gb3^+$ MDCK cells surrounded by wt MDCK cells are shown. (b) – (d) Time course of transcytosed StxB quantified from the signal of apical surface staining with streptavidin-Alexa647 (b), total StxB determined from the signal of StxB-biotin-Alexa488 (c) and the transcytosis efficiency calculated from the ratio of surface staining signal and the total StxB signal (d). To calculate the time courses, signals from at

least 30 cells per condition were quantified from the microscopy data. The graphs show the average from three independent experiments, the error bars represent the SEM.

3.4 The transcytotic route of StxB from the basolateral to the apical plasma membrane

When internalized from the basolateral plasma membrane, StxB first co-localized with EE (Figs. 4a and S4), showing a peak in co-localization at 15 min, which is similar as in the case of apically applied StxB (Fig. 2a). The co-localization with ARE peaked only after 30 min of internalization (Figs. 4b and S5), slightly later as for apically applied StxB (Fig. 2b). This indicates that StxB, which was internalized from the basolateral side, got access to ARE after approximately 30 min, which can also act as exocytic compartment for apical delivery [27,29,39]. Similar as before (Fig. 2c), approximately 50% of basolaterally internalized StxB took the retrograde transport route to the Golgi apparatus (Figs. 4c and S6).

In order to verify the role of ARE as apical exocytic compartment during basolateral to apical STxB transcytosis, we carried out overexpression of wt Rab11a-mCherry and dominant negative Rab11a-S25N-mCherry. For these experiments we had to slightly modify the transcytosis assay. To ensure that all $Gb3^+$ cells were also positive for the Rab11a-variants, a monolayer of wt MDCK cells was transiently co-transfected with Gb3 synthase and Rab11a-plamids according to established protocols [29]. This resulted in single isolated cells within the monolayer that expressed Gb3 as well as the Rab11a-variants (Fig. 4d). To maximize the transcytosis signal, we did not wash out StxB in these experiments, but left StxB in the basolateral compartment during the whole incubation period. As can be seen in Fig. 4e, overexpression of wt-Rab11a-mCherry lowered the amount of StxB that was able to transcytose from the basolateral to the apical plasma membrane to 20% after 30 min and 29 % after 60 min compared to cells that were only transfected with Gb3 synthase. Such an effect of overexpression of wt-Rab11a has also been observed for apical biosynthetic delivery [29], and suggests that Rab11a and ARE play a role in basolateral to apical transcytosis of StxB. Importantly, overexpression of Rab11a-S25N-mCherry completely blocked basolateral to apical transcytosis of StxB (Fig. 4e). Neither overexpression of wt-Rab11a-mCherry nor Rab11a-S25N-mCherry interfered with the uptake of StxB from the basolateral plasma membrane (Fig. 4f). Thus, also the transcytosis efficiencies (Fig. 4g) followed the same trend as the signal from transcytosed StxB. This proves that functional Rab11a and ARE are required for apical delivery of StxB during basolateral to apical transcytosis.

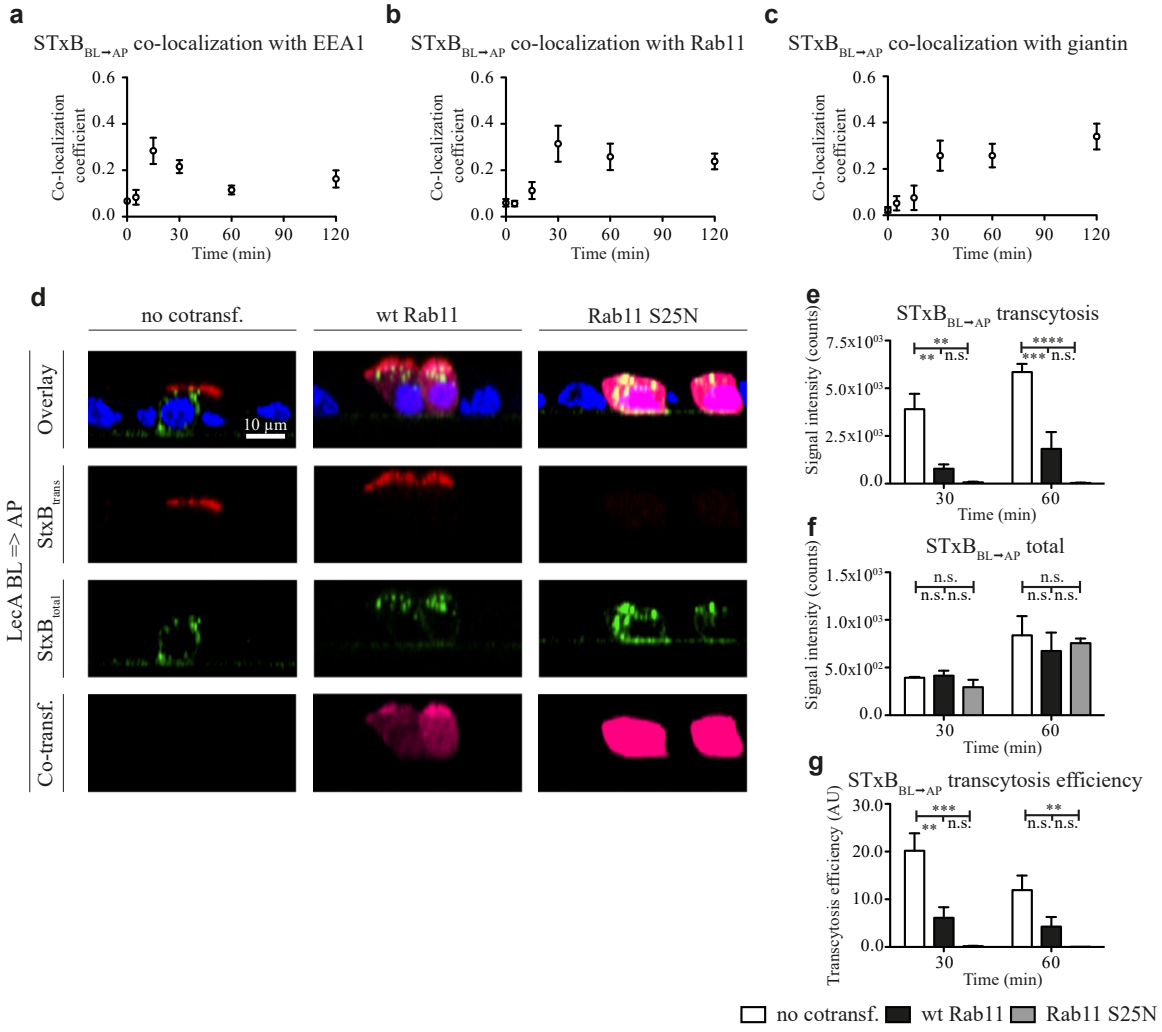

Figure 4: Intracellular trafficking of basolaterally applied StxB.
(a) – (c) StxB-Cy3 was pre-bound to the basolateral (BL) surface at 4°C, followed by incubation at 37°C for the indicated time periods. After fixation and permeabilization intracellular compartment markers (EEA1 in (a), Rab11 in (b), and giantin in (c)) were stained. Representative confocal images for each condition are shown in Figs. S4 - S6, respectively. From the confocal data, the Manders m1 co-localization coefficients, representing the fraction of StxB co-localizing with a compartment marker were calculated. The graphs show the time courses of the averaged co-localization coefficients from n ≥ 3 individual experiments, the error bars represent the SEM. (d) A monolayer of wt MDCK cells was transiently transfected with Gb3 synthase alone (no cotransf.), Gb3 synthase and wild type Rab11a-mCherry (wt Rab11), and Gb3 synthase and dominant negative Rab11a-S25N-mCherry (Rab11 S25N). StxB-biotin-Alexa488 was applied to the basolateral plasma membrane and incubated for 1 h at 37°C. StxB arriving at the apical (AP) plasma membrane was stained with streptavidin-Alexa647. Representative apico-basal cross-sections are shown for each condition in (d). (e) – (g) Quantifications of the experiments presented in (d). Transcytosed StxB was determined from the signal of apical surface staining with streptavidin-Alexa647 (e), total StxB was obtained from the signal of StxB-biotin-Alexa488 (f) and the transcytosis efficiency was calculated from the ratio of surface staining signal to the total StxB signal (g). The average values from three

independent experiments are shown, error bars represent the SEM. * $p<0.05$, ** $p<0.01$, *** $p<0.001$, and n.s. not significant

3.5 Gb3 also drives transcytosis of LecA

The *Pseudomonas aeruginosa* lectin LecA is also able to bind the glycosphingolipid Gb3 [24]. LecA possesses less primary amines than StxB, thus, NHS-ester-based bioconjugation of both, a fluorescent dye and biotin, was not possible with LecA. Therefore, LecA-biotin was utilized and the total amount of bound and internalized LecA was detected by streptavidin-Alexa488 labelling in fixed and permeabilized cells after the transcytosis experiments.

As depicted in Fig. 5a, LecA underwent transcytosis in both directions. Detectable transcytosis signals were seen for the apical to basolateral direction after 30 min (Fig. 5b) and *vice versa* after 60 min (Fig. 5e). A larger number of LecA molecules bound to the apical side than to the basolateral side (Figs. 5c vs. 5f). This is most likely due to the higher steady-state concentration of Gb3 at the apical side, which has also been observed during the StxB transcytosis experiments (Figs. 1c and 3c). Interestingly, the transcytosis efficiencies in both directions did not saturate after 60 min of transport (Fig. 5d for apical to basolateral transcytosis and Fig. 5g for basolateral to apical transcytosis) as has been observed before for StxB (Figs. 1d and 3d).

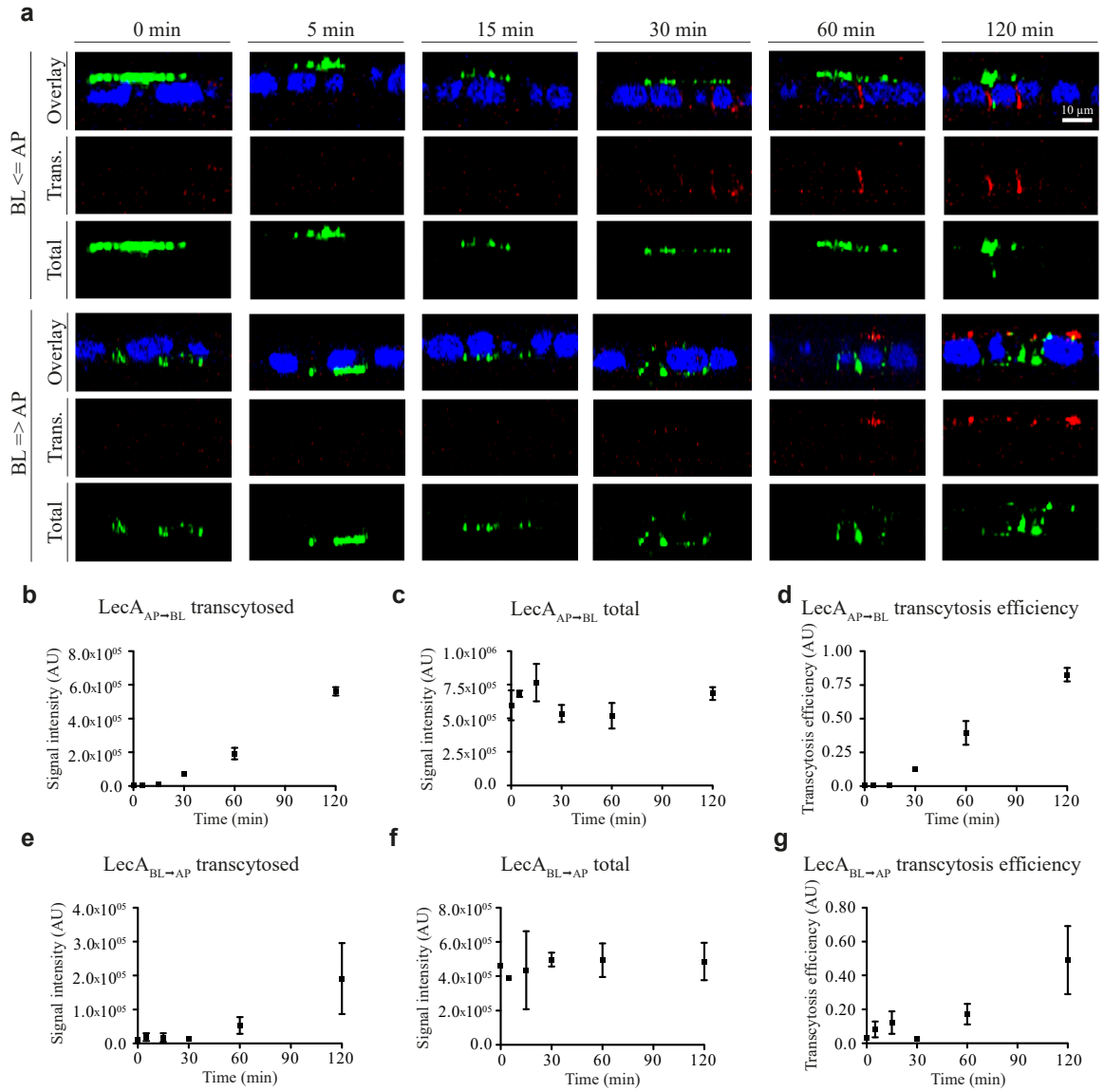

Figure 5: LecA is transcytosed in both directions

(a) - (b) After pre-binding of LecA-biotin for 30 min at 4°C to the apical (AP) plasma membrane (a) or the basolateral (BL) plasma membrane (b), the cells were shifted to 37°C for the indicated time periods. Then, transcytosed LecA was visualized by staining with streptavidin-Alexa647 (red) at the basolateral (a) or the apical (b) cell surface. After fixation and permeabilization, intracellular LecA was stained with streptavidin-Alexa488 (green) and nuclei were counterstained with DAPI (blue). The cells were imaged with a confocal microscope and representative apico-basal cross-sections of $Gb3^+$ MDCK cells surrounded by wt MDCK cells are shown. (b) – (d) Time course of LecA transcytosed in the apical to basolateral direction determined from the signal of basolateral surface staining with streptavidin-Alexa647 (b), total LecA defined by the signal of streptavidin-Alexa488 (c) and the transcytosis efficiency calculated from the ratio of surface staining signal to the total LecA signal (d). (e) – (g) Same experiment as in (b) – (d), but LecA-biotin was applied to the basolateral side and transcytosis was detected on the apical side. The graphs show the average from three independent experiments, the error bars represent the SEM. Within each experiment, the signals from at least 30 cells per condition were quantified.

3.6 Unlike StxB, LecA is not retrogradely transported

Also for LecA transcytosis, we performed a co-localization analysis to investigate the intracellular trafficking route. Apically applied LecA showed a clear co-localization with EE after 15 min, which remained high until the end of the experiment after 120 min (Figs. 6a and S7). The co-localization with ARE peaked at 15 min (Figs. 6b and S8). This behaviour is different from that observed for apically applied StxB (Fig. 2), suggesting differences in intracellular trafficking between LecA and StxB. Indeed, apically applied LecA did not efficiently reach the Golgi apparatus (Figs. 6c and S9), thus suggesting that only a minor fraction of LecA (<15%) is retrogradely transported. Basolaterally applied LecA showed a very slow increase in co-localization with EE (Figs. 6d and S10) and ARE (Figs. 6e and S11), which is again different than the behaviour seen for basolaterally applied StxB (Fig. 4). Also from the basolateral side LecA was not able to efficiently reach the Golgi apparatus (Figs. 6f and S12).

Moreover, we investigated if ARE act as apical exocytic compartment in basolateral to apical transcytosis of LecA. This is indeed the case, as can be seen in Figs. 6g-6j. Similar as for StxB (Figs. 4d-4g), overexpression of Rab11a-S25N-mCherry drastically inhibited apical arrival of basolaterally applied LecA.

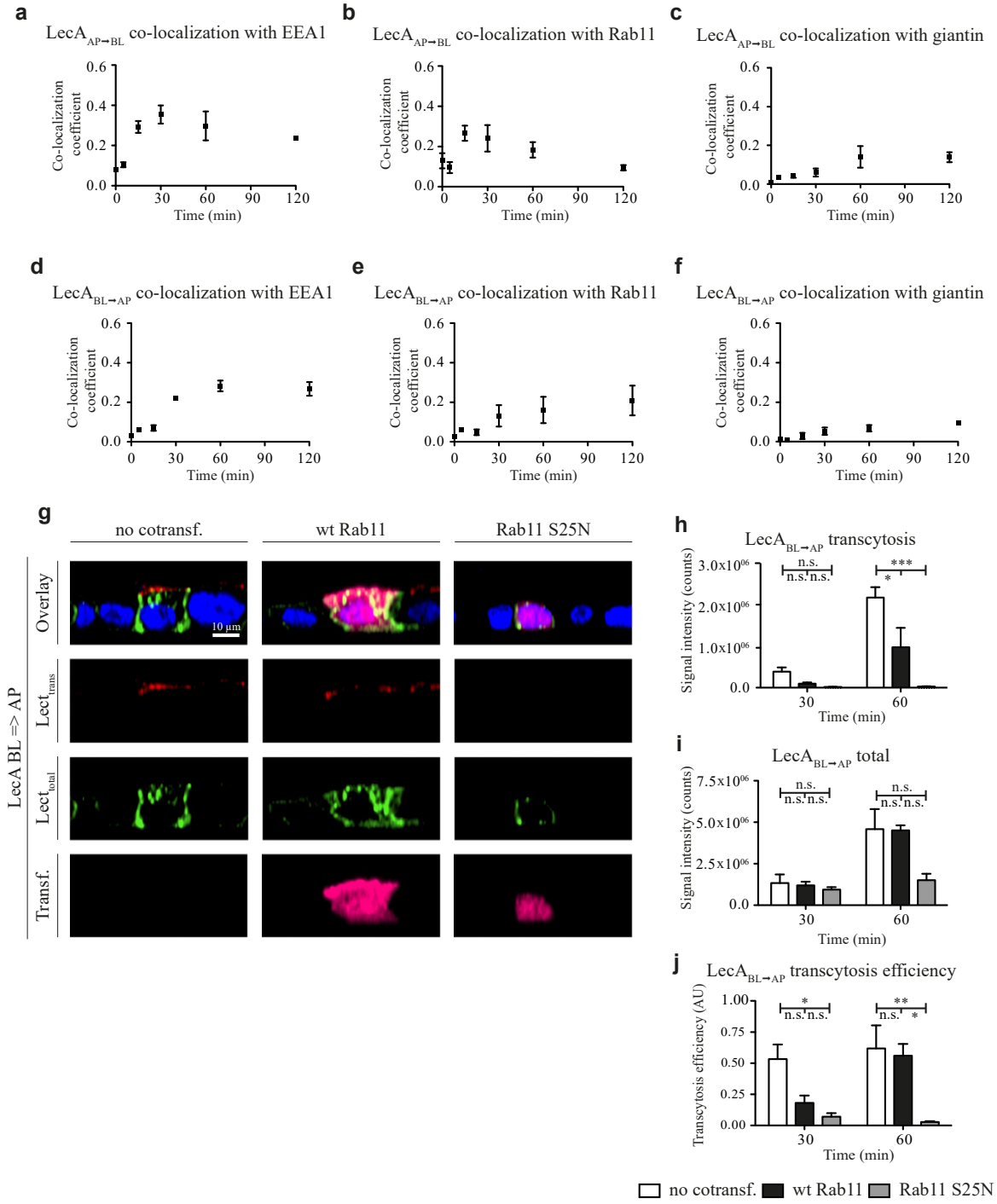

Figure 6: Intracellular trafficking of LecA.
(a) – (c) After LecA-Cy3 was pre-bound to the basolateral surface of the cells (30 min at 4°C), trafficking was enabled by incubation at 37°C for the indicated time periods. After fixation, intracellular compartment markers were co-stained (EEA1 in (a), Rab11 in (b), and giantin in (c)) and cells were imaged with a confocal microscope. Representative micrographs for each condition are shown in Figs. S7 - S9, respectively. (d) – (g) Same experiment as in (a) – (c), but LecA-Cy3 was applied to the basolateral side (Representative confocal micrographs for each condition are presented in Figs. S10 - S12, respectively.). For the figures (a) - (f) the co-localization of LecA with a compartment marker was quantified with a custom-written Matlab program. The graphs show the time

course of the averaged co-localization coefficients from 3 individual experiments, the error bars represent the SEM. (g) A monolayer of wt MDCK cells was transiently transfected with Gb3 synthase alone (no cotransf.), Gb3 synthase and wild type Rab11a-mCherry (wt Rab11), and Gb3 synthase and dominant negative Rab11a-S25N-mCherry (Rab11 S25N). LecA-biotin was applied to the basolateral plasma membrane and incubated for 1 h at 37°C. Afterwards, streptavidin-Alexa647 was applied to the apical plasma membrane to stain transcytosed LecA. Total LecA was detected with streptavidin-Alexa488 after fixation and permeabilization of the cells. Representative cells are shown in apico-basal cross-sections. (h) – (j) Quantifications of the experiment presented in (g). The signal of the apical surface staining with streptavidin-Alexa647 determined transcytosed LecA in (h), total LecA levels were derived from the signal of streptavidin-Alexa488 in (i) and the transcytosis efficiency was calculated from the ratio of surface staining signal to the total LecA signal in (j). The average values from three independent experiments are shown, error bars represent the SEM. * $p<0.05$, ** $p<0.01$, *** $p<0.001$, and n.s. not significant

3.7 StxB and LecA segregate into distinct membrane microdomains during their endocytosis

The experiments before showed that although StxB and LecA were both transcytosed, their intracellular transport was different. Whereas approximately 50% of StxB took the retrograde transport route to the Golgi apparatus, less than 15% of LecA did appear at the Golgi apparatus. Therefore, we investigated when during the transport a separation between LecA and StxB could occur. To this end, we pre-bound StxB-Alexa488 and LecA-Alexa647 to $Gb3^+$ MDCK cells at 4°C and shifted the temperature to 37°C for short time periods to shed light on the early events during endocytosis (Fig. 7). Even when internalization was prohibited, a partial segregation in distinct plasma membrane domains between LecA and StxB was observed (Fig. 7, 0 min). The segregation became clearer after 2 min of incubation at 37°C, and after 15 min vesicles appeared that showed separate LecA- and StxB-domains together with vesicles that were positive for only one of the two lectins. This suggests that, despite binding to the same lipid receptor, LecA and StxB segregate into different membrane domains that after endocytosis enter partially different intracellular trafficking routes.

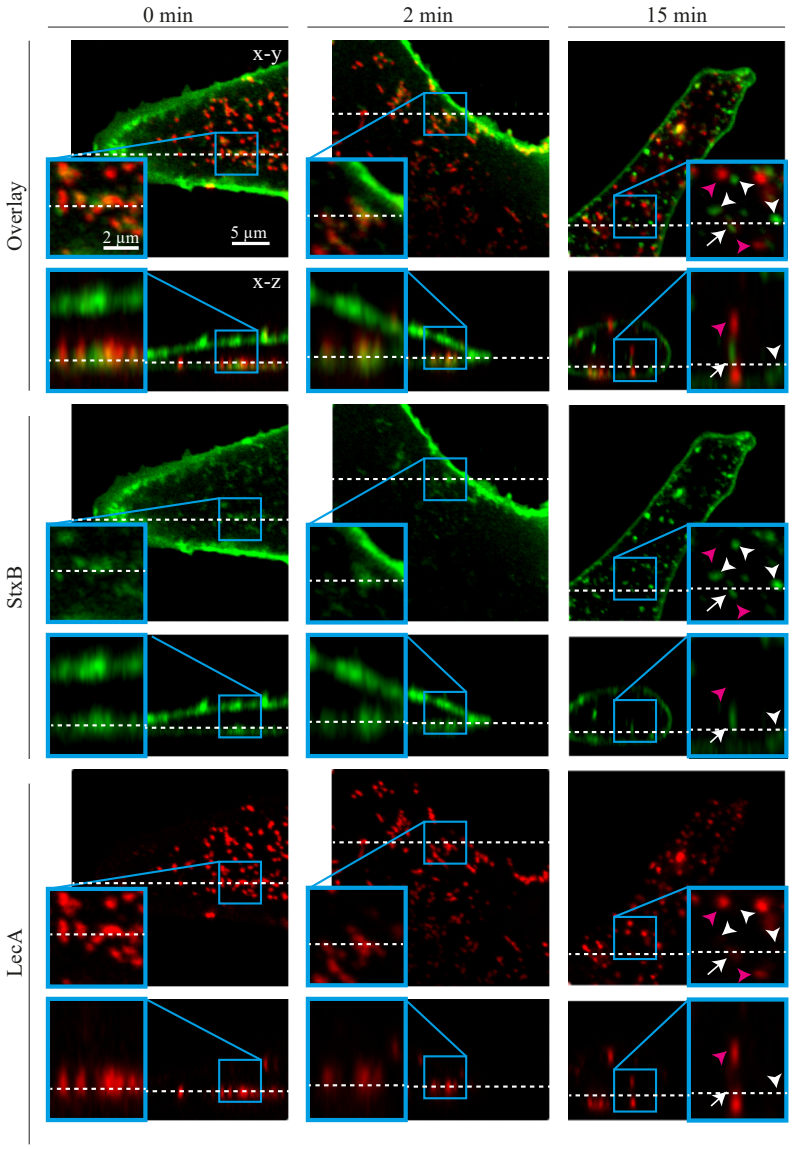

Figure 7: StxB and LecA segregate into separate domains during endocytosis.
StxB-Alexa488 (green) and LecA-Alexa647 (red) were pre-bound to non-polarized $Gb3^+$ MDCK cells at 4°C for 30 min. Then, the cells were heated to 37°C for 0 – 15 min. After fixation, cells were imaged with a confocal microscope. For each condition, a representative x-y cross-section and a corresponding x-z cross-section are shown. White dashed lines indicate the localization of the cross-sections. Zoom-ins from the areas marked with blue squares are also displayed. In the 15 min images, white arrowheads mark vesicles positive only for StxB-Alexa488, magenta arrowheads mark vesicles positive only for LecA-Alexa647, and white arrows mark vesicles showing both, StxB-Alexa488- and LecA-Alexa647-domains.

4 Discussion

Our experiments showed that the two Gb3-binding lectins StxB and LecA undergo transcytosis in a BBB model based on polarized $Gb3^+$ MDCK cells. Transcytotic transport was possible in both directions, from the apical to the basolateral side and *vice versa*. In both directions, transcytosis was mediated by vesicular trafficking, because the lectins reappeared at the opposite surface in a membrane-bound form.

The first step for transcytosis in both directions was the internalization into EE. Then, the lectins populated the recycling system at the side from which they were internalized, until a fraction escaped to the vesicular trafficking system feeding the opposite plasma membrane. This is best illustrated for basolateral to apical transcytosis. After basolateral internalization and co-localization with EE on the basolateral side, the lectins reached the apical trafficking system and arrived at ARE. This compartment has been shown to be involved in apical recycling and apical biosynthetic trafficking [29]. A crucial role for ARE in basolateral to apical receptor-mediated transcytosis has also been found for transcytosis of immunoglobulin A mediated by the polymeric immunoglobulin receptor [39,40]. In line with these observations, we could show that inhibition of ARE by overexpression of dominant negative Rab11a-S25N-mCherry prevented arrival of basolaterally applied lectins at the apical plasma membrane. Together with the established role of ARE in transcytosis via protein-based receptors, our finding that ARE are implicated in transcytosis via lipid-based receptors suggest that ARE are a central hub for most, if not all, basolateral to apical vesicular transcytosis pathways.

Despite the fact that StxB and LecA both bind Gb3, their transcytosis kinetics was different. In addition, approximately 50% of StxB that bound to the apical or basolateral plasma membrane at 4°C was retrogradely transported to the Golgi apparatus. In contrast to that, only <15% of LecA was retrogradely transported. This observation suggests that LecA is preferably transcytosed, whereas only a fraction of StxB does that. In line with the idea that a larger fraction of LecA is available for transcytosis, we observed that the transcytosis efficiency of StxB saturated after approximately 60 min, whereas the transcytosis efficiency of LecA showed no saturation within our measurement period of 120 min. During an infection with bacteria secreting Shiga toxin, for example upon intestinal colonization with enterohemorrhagic *Escherichia coli* (EHEC) [41], the toxin does not only affect cells at the site of infection, but efficiently spreads to other tissues to reach the kidney and the CNS, where it inflicts severe damage [21]. It is interesting to note that this spread requires initial transcytosis across the intestinal epithelium, which has been

suggested to occur through macropinocytosis because this tissue is Gb3-negative in healthy humans [41]. However, to reach the CNS, subsequent transport across endothelia including the BBB, which express Gb3 [19–21], is required. This latter transcytosis most likely occurs through the Gb3-dependent pathway we describe here, because the macropinocytotic activity of the BBB is very low [42]. Nevertheless, it seems that StxB has evolved to be able to do both: spreading, which requires transcytosis, and cell intoxication, which requires retrograde transport. Our model system replicates this dual nature of Shiga toxin intracellular transport. The molecular mechanism for this differential StxB transport is not well understood. It has been shown that the degree of saturation, length, and hydroxylation of Gb3 acyl chains influences the internalization [18] as well as the intracellular transport route of STxB [43,44]. A similar observation has been made by Saslowsky et al. for the transcytosis of cholera toxin (Ctx), which binds to the glycosphingolipid monosialotetrahexosylganglioside (GM1) [45]. They demonstrated that Ctx was also able to undergo transcytosis as well as retrograde transport, however, the portion of Ctx that was transcytosed bypassed the retrograde transport route. In addition, the authors showed that only GM1 species that contained *cis*-unsaturated or short acyl chains in the ceramide domain were able to transcytose from the apical to the basolateral plasma membrane [45]. Taken together, the virtual absence of retrograde transport for LecA in our model system suggests that LecA has a preference for different Gb3 species than StxB. This would result in sorting of the two lectins, which we indeed have observed already during endocytosis. A detailed investigation if LecA and StxB preferentially bind different Gb3 species is currently ongoing at our laboratory.

The absence of retrograde trafficking for LecA makes this lectin an attractive candidate for transcellular drug delivery, because in this case retrograde transport is not desired. In particular, LecA would be an interesting carrier for drug delivery across the BBB, because, as mentioned before, this endothelium expresses Gb3 [19–21]. In this context it is interesting to note that TNF-alpha treatment additionally enhanced Gb3 expression in both human macrovascular umbilical vein endothelial cells and human microvascular brain endothelial cells [20]. This suggests that Gb3 expression can be boosted in target tissues with appropriate co-stimulation.

5 Conclusions

In this study, we investigated glycosphingolipid-specific lectins for their suitability as carriers for drug delivery over barriers like the BBB. We found that two lectins that bind

Gb3, StxB and LecA, are both able to undergo transcytosis in an *in vitro* model system of the BBB based on $Gb3^+$ MDCK cells. We unravelled the trafficking route of both lectins by quantifying the sequential co-localization with intracellular compartments. We found that both lectins reach EE after internalization and that ARE are central exocytic compartments during basolateral to apical transcytosis. Whereas StxB underwent both, retrograde transport as well as transcytosis, LecA did not enter the retrograde transport route. This makes LecA a promising candidate for transcellular drug delivery that can be combined with established strategies, like coupling LecA to porous nanoparticles or polymers that carry drugs incorporated in their matrix [46–48], or coupling drugs to LecA via an enzymatically cleavable linker [49,50]. In addition, these findings demonstrate that lectins with structurally different binding pockets for the same glycosphingolipid receptor can take different intracellular trafficking routes. This suggests that there is the possibility to engineer lectins that sort themselves into the desired trafficking pathway for drug delivery. Taken together, we propose glycosphingolipids as promising new class of endogenous receptors that can be used for efficient lectin-based transcellular drug delivery.

6 Acknowledgments

W.R. acknowledges support by the Excellence Initiative of the German Research Foundation (EXC 294), the Baden-Württemberg Stiftung (Zukunftsoffensive IV Innovation und Exzellenz), a German Research Foundation grant (RO 4341/2-1), and a starting grant from the European Research Council (Programme “Ideas”, ERC-2011-StG 282105).

7 References

[1] W.M. Pardridge, The blood-brain barrier: Bottleneck in brain drug development, NeuroRX. 2 (2005) 3–14. doi:10.1602/neurorx.2.1.3.

[2] N.J. Abbott, Astrocyte-endothelial interactions and blood-brain barrier permeability, J. Anat. 200 (2002) 629–638. doi:10.1046/j.1469-7580.2002.00064.x.

[3] K. Hatherell, P.-O. Couraud, I. a Romero, B. Weksler, G.J. Pilkington, Development of a three-dimensional, all-human in vitro model of the blood-brain barrier using mono-, co-, and tri-cultivation Transwell models., J. Neurosci. Methods. 199 (2011) 223–9. doi:10.1016/j.jneumeth.2011.05.012.

[4] M.J. Coloma, H.J. Lee, A. Kurihara, E.M. Landaw, R.J. Boado, S.L. Morrison, et al., Transport across the primate blood-brain barrier of a genetically engineered chimeric monoclonal antibody to the human insulin receptor., Pharm. Res. 17 (2000) 266–74. doi:10.1023/A:1007592720793.

[5] J.D. Huber, R.D. Egleton, T.P. Davis, Molecular physiology and pathophysiology of tight junctions in the blood-brain barrier., Trends Neurosci. 24 (2001) 719–725. doi:10.1016/S0166-2236(00)02004-X.

[6] Q. Wang, J.D. Rager, K. Weinstein, P.S. Kardos, G.L. Dobson, J. Li, et al., Evaluation of the MDR-MDCK cell line as a permeability screen for the blood-brain barrier., Int. J. Pharm. 288 (2005) 349–59. doi:10.1016/j.ijpharm.2004.10.007.

[7] M. von Wedel-Parlow, P. Wölte, H.-J. Galla, Regulation of major efflux transporters under inflammatory conditions at the blood-brain barrier in vitro., J. Neurochem. 111 (2009) 111–8. doi:10.1111/j.1471-4159.2009.06305.x.

[8] P. Garberg, M. Ball, N. Borg, R. Cecchelli, L. Fenart, R.D. Hurst, et al., In vitro models for the blood-brain barrier., Toxicol. In Vitro. 19 (2005) 299–334. doi:10.1016/j.tiv.2004.06.011.

[9] K.A. Youdim, M.Z. Qaiser, D.J. Begley, C.A. Rice-Evans, N.J. Abbott, Flavonoid permeability across an in situ model of the blood-brain barrier, Free Radic. Biol. Med. 36 (2004) 592–604. doi:10.1016/j.freeradbiomed.2003.11.023.

[10] H. Fischer, R. Gottschlich, A. Seelig, Blood-brain barrier permeation: Molecular parameters governing passive diffusion, J. Membr. Biol. 165 (1998) 201–211.

doi:10.1007/s002329900434.

[11] Y. Chen, L. Liu, Modern methods for delivery of drugs across the blood-brain barrier, Adv. Drug Deliv. Rev. 64 (2012) 640–665. doi:10.1016/j.addr.2011.11.010.

[12] J. Niewoehner, B. Bohrmann, L. Collin, E. Urich, H. Sade, P. Maier, et al., Increased Brain Penetration and Potency of a Therapeutic Antibody Using a Monovalent Molecular Shuttle, Neuron. 81 (2014) 49–60. doi:10.1016/j.neuron.2013.10.061.

[13] Z.M. Qian, H. Li, H. Sun, K. Ho, Targeted Drug Delivery via the Transferrin Receptor-, 54 (2002) 561–587.

[14] D. Wu, J. Yang, W.M. Pardridge, Drug targeting of a peptide radiopharmaceutical through the primate blood-brain barrier in vivo with a monoclonal antibody to the human insulin receptor, J. Clin. Invest. 100 (1997) 1804–1812. doi:10.1172/JCI119708.

[15] H. Sade, C. Baumgartner, A. Hugenmatter, E. Moessner, P.O. Freskgard, J. Niewoehner, A human blood-brain barrier transcytosis assay reveals antibody transcytosis influenced by pH-dependent receptor binding, PLoS One. 9 (2014). doi:10.1371/journal.pone.0096340.

[16] I. Van Genderen, G. Van Meer, Differential targeting of glucosylceramide and galactosylceramide analogues after synthesis but not during transcytosis in Madin-Darby canine kidney cells, J. Cell Biol. 131 (1995) 645–654. doi:10.1083/jcb.131.3.645.

[17] K. Simons, G. Van Meer, Lipid Sorting in Epithelial Cells, Biochemistry. 27 (1988) 6197–6202. http://pubs.acs.org/doi/abs/10.1021/bi00417a001 (accessed February 11, 2014).

[18] W. Römer, L. Berland, V. Chambon, K. Gaus, B. Windschiegl, D. Tenza, et al., Shiga toxin induces tubular membrane invaginations for its uptake into cells., Nature. 450 (2007) 670–5. doi:10.1038/nature05996.

[19] I. Meisen, R. Rosenbrück, H. Galla, Expression of Shiga toxin 2e glycosphingolipid receptors of primary porcine brain endothelial cells and toxin-mediated breakdown of the blood-brain barrier, …. (2013) 1–61. http://glycob.oxfordjournals.org/content/early/2013/02/21/glycob.cwt013.short

(accessed May 2, 2013).

[20] P.B. Eisenhauer, P. Chaturvedi, R.E. Fine, A.J. Ritchie, J.S. Pober, T.G. Cleary, et al., Tumor Necrosis Factor Alpha Increases Human Cerebral Endothelial Cell Gb 3 and Sensitivity to Shiga Toxin, Infect. Immun. 69 (2001) 1889–1894. doi:10.1128/IAI.69.3.1889.

[21] L. Johannes, W. Römer, Shiga toxins--from cell biology to biomedical applications., Nat. Rev. Microbiol. 8 (2010) 105–16. doi:10.1038/nrmicro2279.

[22] F. Mallard, C. Antony, D. Tenza, J. Salamero, B. Goud, L. Johannes, Direct Pathway from Early/Recycling Endosomes to the Golgi Apparatus Revealed through the Study of Shig Toxin B-fragment Transport, 143 (1998) 973–990.

[23] J.E. McKenzie, The recycling endosome is required for transport of retrograde toxins, Thesis. (2013) 1–111.

[24] T. Eierhoff, B. Bastian, R. Thuenauer, J. Madl, A. Audfray, S. Aigal, et al., A lipid zipper triggers bacterial invasion., Proc. Natl. Acad. Sci. U. S. A. 111 (2014) 6–11. doi:10.1073/pnas.1402637111.

[25] A. Imberty, M. Wimmerová, E.P. Mitchell, N. Gilboa-Garber, Structures of the lectins from Pseudomonas aeruginosa: insights into the molecular basis for host glycan recognition, Microbes Infect. 6 (2004) 221–228. doi:10.1016/j.micinf.2003.10.016.

[26] E. Rodriguez-Boulan, I.G. Macara, Organization and execution of the epithelial polarity programme, Nat. Rev. Mol. Cell Biol. 15 (2014) 225–242. doi:10.1038/nrm3775.

[27] J.R. Goldenring, Recycling endosomes., Curr. Opin. Cell Biol. 35 (2015) 117–122. doi:10.1016/j.ceb.2015.04.018.

[28] D.M. Bryant, K.E. Mostov, From cells to organs: building polarized tissue., Nat. Rev. Mol. Cell Biol. 9 (2008) 887–901. doi:10.1038/nrm2523.

[29] R. Thuenauer, Y. Hsu, J.M. Carvajal-Gonzalez, S. Deborde, J. Chuang, W. Römer, et al., Four-dimensional live imaging of apical biosynthetic trafficking reveals a post-Golgi sorting role of apical endosomal intermediates., Proc. Natl. Acad. Sci. U. S. A. 111 (2014) 4127–32. doi:10.1073/pnas.1304168111.

[30] V. Zinchuk, O. Zinchuk, T. Okada, Quantitative colocalization analysis of multicolor confocal immunofluorescence microscopy images: pushing pixels to explore biological phenomena., Acta Histochem. Cytochem. 40 (2007) 101–111. doi:10.1267/ahc.07002.

[31] J.M. Wilson, M. de Hoop, N. Zorzi, B.H. Toh, C.G. Dotti, R.G. Parton, EEA1, a tethering protein of the early sorting endosome, shows a polarized distribution in hippocampal neurons, epithelial cells, and fibroblasts., Mol. Biol. Cell. 11 (2000) 2657–71. http://www.pubmedcentral.nih.gov/articlerender.fcgi?artid=14947&tool=pmcentrez&rendertype=abstract.

[32] E. Rodriguez-Boulan, G. Kreitzer, A. Müsch, Organization of vesicular trafficking in epithelia., Nat. Rev. Mol. Cell Biol. 6 (2005) 233–47. doi:10.1038/nrm1593.

[33] F. Mallard, B.L. Tang, T. Galli, D. Tenza, A. Saint-Pol, X. Yue, et al., Early/recycling endosomes-to-TGN transport involves two SNARE complexes and a Rab6 isoform., J. Cell Biol. 156 (2002) 653–64. doi:10.1083/jcb.200110081.

[34] D.R. Sheff, E.A. Daro, M. Hull, I. Mellman, The Receptor Recycling Pathway Contains Two Distinct Populations of Early Endosomes with Different Sorting Functions, J. Cell Biol. 145 (1999) 123–139. doi:10.1083/jcb.145.1.123.

[35] J.E. McKenzie, B. Raisley, X. Zhou, N. Naslavsky, T. Taguchi, S. Caplan, et al., Retromer guides STxB and CD8-M6PR from early to recycling endosomes, EHD1 guides STxB from recycling endosome to Golgi., Traffic. 13 (2012) 1140–59. doi:10.1111/j.1600-0854.2012.01374.x.

[36] R. Rojas, G. Apodaca, Immunoglobulin transport across polarized epithelial cells., Nat. Rev. Mol. Cell Biol. 3 (2002) 944–55. doi:10.1038/nrm972.

[37] T. Falguières, F. Mallard, C. Baron, D. Hanau, C. Lingwood, B. Goud, et al., Targeting of Shiga Toxin B-Subunit to Retrograde Transport Route in Association with Detergent-resistant Membranes, 12 (2001) 2453–2468.

[38] M. Warnier, W. Römer, J. Geelen, J. Lesieur, M. Amessou, L. van den Heuvel, et al., Trafficking of Shiga toxin/Shiga-like toxin-1 in human glomerular microvascular endothelial cells and human mesangial cells., Kidney Int. 70 (2006) 2085–91. doi:10.1038/sj.ki.5001989.

[39] T. Su, D.M. Bryant, F. Luton, M. Vergés, S.M. Ulrich, K.C. Hansen, et al., A kinase cascade leading to Rab11-FIP5 controls transcytosis of the polymeric immunoglobulin receptor, Nat. Cell Biol. 12 (2010) 1143–1153. doi:10.1038/ncb2118.

[40] G. Apodaca, A. Leonid, E. Mostov, Receptor-mediated Transcytosis of IgA in MDCK Cells Is via Apical Recycling Endosomes, J. Cell Biol. 125 (1994) 67–86.

[41] M. Laiko, R. Murtazina, I. Malyukova, C. Zhu, E.C. Boedeker, O. Gutsal, et al., Shiga toxin 1 interaction with enterocytes causes apical protein mistargeting through the depletion of intracellular galectin-3., Exp. Cell Res. 316 (2010) 657–66. doi:10.1016/j.yexcr.2009.09.002.

[42] W.A. Banks, Characteristics of compounds that cross the blood-brain barrier., BMC Neurol. 9 Suppl 1 (2009) S3. doi:10.1186/1471-2377-9-S1-S3.

[43] S. Arab, C.A. Lingwood, Influence of phospholipid chain length on verotoxin/globotriaosyl ceramide binding in model membranes: Comparison of a supported bilayer film and liposomes, Glycoconj. J. 13 (1996) 159–166. doi:10.1007/BF00731490.

[44] C.A. Lingwood, Glycosphingolipid functions, Cold Spring Harb. Perspect. Biol. 3 (2011) 1–26. doi:10.1101/cshperspect.a004788.

[45] D.E. Saslowsky, Y.M. te Welscher, D.J.-F. Chinnapen, J.S. Wagner, J. Wan, E. Kern, et al., Ganglioside GM1-mediated transcytosis of cholera toxin bypasses the retrograde pathway and depends on the structure of the ceramide domain., J. Biol. Chem. 288 (2013) 25804–9. doi:10.1074/jbc.M113.474957.

[46] J. Huwyler, D. Wu, W.M. Pardridge, Brain drug delivery of small molecules using immunoliposomes., Proc. Natl. Acad. Sci. U. S. A. 93 (1996) 14164–14169. doi:10.1073/pnas.93.24.14164.

[47] L. Juillerat-Jeanneret, The targeted delivery of cancer drugs across the blood-brain barrier: chemical modifications of drugs or drug-nanoparticles?, Drug Discov. Today. 13 (2008) 1099–1106. doi:10.1016/j.drudis.2008.09.005.

[48] A. Jayagopal, E.M. Sussman, V.P. Shastri, Functionalized solid lipid nanoparticles for transendothelial delivery, IEEE Trans. Nanobioscience. 7 (2008) 28–34. doi:10.1109/TNB.2008.2000147.

[49] R. Reents, D.A. Jeyaraj, H. Waldmann, Enzymatically cleavable linker groups in polymer-supported synthesis, Drug Discov. Today. 7 (2002) 71–76. doi:10.1016/S1359-6446(01)02088-8.

[50] G.M. Dubowchik, M.A. Walker, Receptor-mediated and enzyme-dependent targeting of cytotoxic anticancer drugs, Pharmacol. Ther. 83 (1999) 67–123. doi:10.1016/S0163-7258(99)00018-2.